

2D tracking of *Platynereis dumerilii* worms during spawning

Daniel Pucher, Walter G. Kropatsch, Nicole M. Artner
Pattern Recognition and Image Processing (PRIP)
Vienna University of Technology, Austria
<http://www.prip.tuwien.ac.at>

Stephanie Bannister, Kristin Tessmar-Raible
Max F. Perutz Laboratories
University of Vienna, Austria
<https://www.mfpl.ac.at/>

Abstract. *Platynereis dumerilii* are marine worms that reproduce by external fertilisation and exhibit particular swimming behaviours during spawning. In this paper we propose a novel worm tracking approach that enables the 2D tracking and feature extraction during the spawning process of these worms. The gathered data will be used in the future to characterise and compare male and female spawning behaviours.



Figure 1. Image of a male (red) and female (yellow) worm.

1. Introduction

Platynereis dumerilii are marine polychaete worms (Lophotrochozoa, annelida, nereididae), which swim only when sexually mature, in order to reproduce. The timing of reproductive spawning events in this species is synchronized with the moon phase, whereby spawning in nature occurs primarily during new moon. This together with chemical pheromone signaling allows mature male and female worms to locate one another and engage in spawning behaviors that constitute the nuptial dance. See Figure 1 for an image of a male and female worm.

The spawning behaviors of male and female worms are important for successful fertilization of the gametes. The spawning process consists of four general phases: Pre-spawning, engaged spawning, gamete release and post-spawning. During pre-spawning, male and female worms typically swim independently of one another, usually with lower speeds, and display a linear body shape. Engaged spawning is initiated when male and female

worms come into close contact and sense chemical pheromones secreted into the water by the opposite sex. This is accompanied by a noticeable change in swimming behavior for both sexes: swimming speeds increase (particularly for males), and worms either begin to swim in circles, or swim in tighter circles (particularly for females). Other changes in the plane of swimming are more frequently observed in both sexes during engaged spawning behavior. During gamete release, sperm and eggs are secreted into the water, which particularly for female worms, results in a dramatic change in body area, length and overall shape. The time individual spawning phases take varies and depends on the worms and their willingness to engage. Some worm pairs are better matches than others which can result in shorter spawning phases.

Our goal is to analyse these spawning behaviours in a quantitative manner, and to characterise and compare male and female-specific spawning behaviours.

2. Task formulation

The aim is to develop methods that enable the tracking of spawning worms from captured videos and extract features to quantify behaviours. For the tracking, it is important that we distinguish male and female worms in every frame of a captured video, label them and keep track of those labels. This paper focuses on the extraction of features for the analysis of behaviours. The tracking task is simplified by only considering videos with single worms. In order to quantify behaviours, we currently extract the following worm features:

1. *Skeleton*

The skeleton describes the center line of a worm and is defined by two endpoints and an ordered list of points between them. We use the skeleton to calculate the curvature of a worm and to generate a normalized shape representation.

2. *Head position*

The head position is an important feature for the calculation of the velocity and the worm trajectory. We define it as an endpoint of the skeleton. The tangent of the skeleton in this endpoint can give us information on the orientation of the worm.

To choose the right endpoint, we currently select it at the beginning of a video and keep track of that selection.

3. *Velocity*

As the swimming speeds increase for both sexes, the velocity is a good indication for the beginning of the engaged spawning.

4. *Trajectory of the worm head*

The mapping of the swimming trajectories gives us information on the interaction between two worms. Furthermore, for individual worms, the curvature of the trajectory can be compared to the curvature of the worm. A high correlation indicates a circular movement and increases the robustness of the curvature estimation. The trajectory can also give an indication on where we can expect the worm to be in a following frame.

5. *Curvature*

Measurements of body curvature tell us both about the gross and fine body movements

of the worm during the different spawning phases. The gross curvature of the worm's body in general provides information on the directionality of swimming. For example, a mostly straight linear profile would be indicative of linear swimming, while smoothly curved body profiles would indicate circular swimming. Good resolution of finer-scale body curvatures along the length of the worm is also important. For example, a linear profile with several bends could indicate an acceleration of swim speed, or 'wriggling' movements, depending on the amplitude of the curvatures. Such wriggling movements can be seen for males when they are stopping to secrete sperm. Similarly, as gametes are released from the tail, mapping fine-scale curvatures at the tip of the tail could be used to map gamete release events, or characterize sex-specific gamete release behaviours. For example, we have observed fast small tail flicks in males during sperm release, and curling of the tip of the tail in females just prior to egg release. The calculation of the curvature is based on the skeleton of the worm.

6. *Normalized shape*

To make the comparison of different worms (or of the same worm at different times in a video) easier, we create normalized shape representations. To do this we follow a recent strategy which is known as co-registration where shapes are first straightened or flattened to then register different views/deformations of the same normalized shape [1].

7. *Length and area*

During the gamete release phase the body length and area changes, especially for female worms. Therefore, these features are a good indicator for the beginning of this phase.

3. Existing tracking approaches

The tracking of animals and the extraction of features to quantify behaviours is not a new field of application. *Caenorhabditis elegans* (*C. elegans*) are roundworms that have been used as model systems in neuroscience for years and the demand for robust computational methods has led to a number of different tracking systems like Nemo

[10], OptoTracker [8] or a tracking system developed by Chatenay and Schafer [2]. These worm trackers are capable of tracking worms and extracting a variety of different features. Unfortunately they are developed for *C. elegans* worms who differ in their appearance as well as their locomotion from *Platynereis dumerilii*. Furthermore some of them are only capable of tracking single worms and others terminate the tracking of animals if they collide and assigns new tracks after they separate again. This does not guaranty a continuous trajectory of a single worm for a whole video sequence, which is an important requirement for our behaviour analysis. Other animal tracking projects like AnTracks (www.antracks.org) or "Visual Ants Tracking" by Ying [11] are capable of tracking animals, but do not allow the extraction of features, which match our requirements.

Therefore, we propose a new system that is capable of tracking *Platynereis dumerilii* worms and offers feature extraction including a new method to compute normalized shape forms.

4. Experimental setup

The setup of our worm tracker consists of a light-tight box, a mounted infrared camera and an ordinary PC to capture the videos. The worms are placed inside a spherical bowl we refer to as arena. Figure 2 shows the arena with two worms.



Figure 2. Image of the arena with two worms taken from a captured video.

The camera takes videos at a size of 1280x960 pixels with 60 frames per second. The infrared camera is important as the spawning in nature occurs at night and we want to reproduce this

environment in the lab. The single camera setup has some limitations regarding 3D movements of the worms, as they might conceal parts of their body from the cameras viewpoint, resulting in a flawed representation. Analysis of spawning videos have shown, that the worms move horizontally near the water surface. Therefore, we decided to use this single camera setup and neglect the few cases where the gathered data is flawed due to 3D movement. Although, we might change the setup in the future using three cameras instead of one to solve the issue with the 3D movement.

5. Segmentation and tracking

Basically, male and female worms can be distinguished by their color and anterior / posterior segment border, which can be seen in Figure 3.

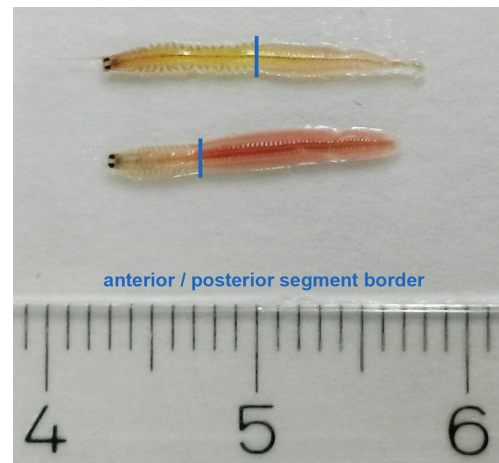


Figure 3. Image of a female (top) and a male (bottom) worm with their segment borders (Scale in cm).

The segment border divides a worm into a head and a tail part and the position of the border is different for male and female worms. Relative to their whole body length, male worms have a longer tail than female worms. Therefore, the segment border is closer to the head. Unfortunately, the segment border is not always clearly visible.

Figure 4 shows three frames of the same worm in the same video just a few seconds apart. These frames illustrate the problem with the segment border. The worms tend to turn sideways when moving fast and in such cases the segment border is not visible to the camera. This prevents us from using the segment border as a feature to distinguish male and female worms.



Figure 4. Three different frames of a single worm taken from the same video just a few seconds apart. In the first frame on the left the worm turned sideways, therefore the segment border is not visible.

Furthermore, due to the infrared capture, we do not have color information in the captured videos and the available grayvalues are not distinctive enough to distinguish male and female worms.

Therefore, we choose an approach that does not rely on the shape and color of the worms, but on their continuous motion over time. First, we label the worms at the beginning of a captured video. Then, we calculate the distance between the head positions in consecutive frames and assign the label based on the smaller deviation. This approach already works well for single worms, but it is too simple to track pairs of worms, as they tend to overlap and the distance of head positions alone is not a robust criteria.

In this paper, we focus on tracking of single worms. We will extend our approach to setups with worm pairs in the future. Although, we only track single worms at the moment, it is still possible to analyse separate spawning behaviours in male and female worms, as we add eggs or sperm manually to the arena and the worms react to them. This allows us to analyse isolated spawning behaviours.

To track a single worm we first need to segment it from the background. We do this with a simple background subtraction for every frame of the video. For the subtraction, it is important that there is at least one frame at the beginning of the video with an empty arena, which serves as the background image. As this image serves as the background image for the whole video, it is assumed that the arena does not move during the video.

After the background subtraction the resulting image is converted to a binary image, based on a global threshold. The binary image gives us a collection of regions that correspond to changes in relation to the empty arena. Ideally there is only

one region for a single worm. Unfortunately, as the worm produces some noise when moving in the arena (particles or bubbles in the water, reflections on the edge of the arena) we also get some noise in our binary image. Therefore, we only consider regions whose area is above a given threshold as worms. As the regions generated by noise are very small, this approach works very well in our current setup.

6. Feature extraction

Features are extracted for every frame of the captured video and are based on the binary region and/or the skeleton of a worm.

6.1. Skeleton

Given the binary region of the worm, we use morphological thinning to compute the skeleton. In our case this approach is superior to the morphological skeletonization with the medial axis transform algorithm as the latter tends to generate more spurious branches. See Figure 5 for a comparison between the two approaches for a sample worm. The thinning approach also tends to create a smoother skeleton.

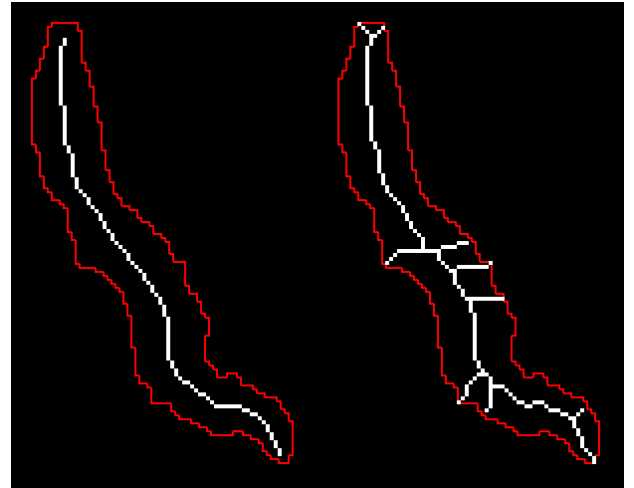


Figure 5. Illustration of the worm skeletons (white) computed from the binary segmentation image (outlined by the red line). The left skeleton was computed using the morphological thinning, the right one using skeletonization (MAT) technique.

The skeleton is defined as an 8-connected curve $s = \langle p_1, \dots, p_n \rangle$ where $p_i = (x_i, y_i)$ with $i = 1, \dots, n$. We order the points p_i of the skeleton from head to tail by comparing the endpoints of the skeleton in one frame with the endpoints in the previous frame. The

position of the head in the first frame of the video has to be specified by the user.

6.2. Head position

As we store the skeleton points in a head to tail order, we get the head position from the first point $p_1 = (x_1, y_1)$ in s .

6.3. Trajectory of the worm head

Given a list of head positions $h = \langle h_1, \dots, h_n \rangle$ where $h_i = (x_i, y_i)$ with $i = 1, \dots, n$ we can generate a connected trajectory. Furthermore, its curvature can be computed to provide information on the swimming direction. Figure 11 shows a section of the trajectory from a single worm video.

6.4. Velocity

Velocity is defined as the rate of change of position with respect to time. We get the change of position by considering the head positions of a single worm in two consecutive frames and calculating the Euclidean distance between the two positions. The time between two frames is given by $1/fps$, where fps is the number frames per second of the video source.

6.5. Curvature

According to Hermann and Klette [6], the estimation of the curvature along a discrete curve can roughly be divided into three categories: the derivative of the tangent angle, the derivative of the curve and the radius of the osculating circle. We chose a method based on osculating circles as it is fast and the implementation is simple. Gray [5] defines the osculating circle of a curve C at a given point P in the continuous space as the circle that has the same tangent as C at point P as well as the same curvature. We approximate these circles with the circumscribed circles of triangles on the discrete skeleton curve. Casey [3] defined the circumscribed circle as the unique circle that passes through each of the triangle's three vertices.

Given the definition for the skeleton s at the beginning of this section, let k be $1 \leq k \leq \lfloor \frac{n}{2} \rfloor$ if n is odd and $1 \leq k \leq (\lfloor \frac{n}{2} \rfloor - 1)$ if n is even, where n is the number of points on the skeleton. For each point p_i on s we define a triangle between the three points p_{i-k} , p_i and p_{i+k} . Then the radius of the triangles circumscribed circle is computed

to calculate the curvature at p_i . See Figure 6 for a visualization.

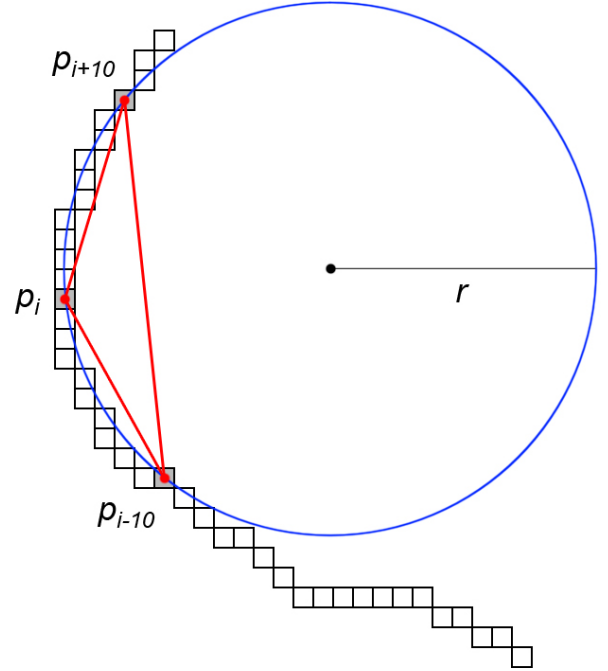


Figure 6. Illustration of the circumscribed circle (blue) for a single point p_i on a skeleton. The circle passes through every vertex of the triangle (red) formed by the points p_{i-k} , p_i and p_{i+k} with $k = 10$.

The radius of the circumscribed circle is defined as $radius = \frac{abc}{4 \cdot area}$, where a, b and c correspond to the edge lengths of the triangle and $area$ is the area of the triangle. The area of a triangle is given by $area = \frac{1}{2} \cdot \text{determinant}$ where $determinant$ refers to the determinant of the triangle matrix, which is formed from the three triangle points:

$$determinant = \begin{vmatrix} x_1 & y_1 & 1 \\ x_2 & y_2 & 1 \\ x_3 & y_3 & 1 \end{vmatrix}$$

As the sign of the determinant gives an indication on the orientation of the triangle and therefore an indication on the direction of the curvature, we don't use the absolute value. So we define the area as $area = \frac{1}{2} \cdot \text{determinant}$. With this information the radius is then defined as $radius = \frac{abc}{2 \cdot \text{determinant}}$. The curvature is given by the inverse of the radius $c = \frac{1}{radius}$. As we do not take the absolute value of the determinant when calculating the radius, the curvature is a signed value that is positive if the curvature is on the right side and negative if the curvature is on the left side of the skeleton curve. See Figure 7 for a visualization.

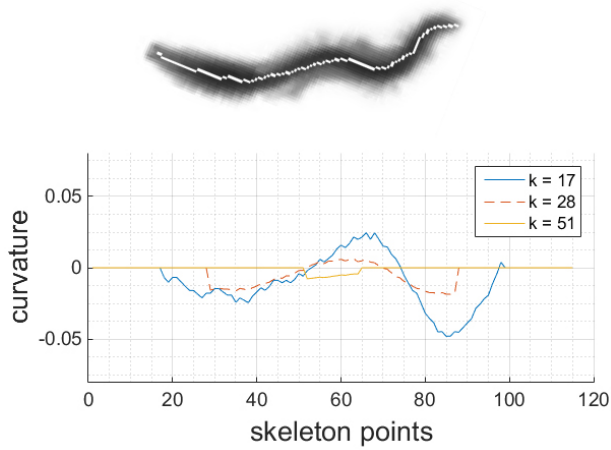


Figure 7. Image of a worm with its skeleton (top) and a plot of the estimated curvature of the worm for different k (bottom).

An important factor in the accuracy of this algorithm is the parameter k that defines a neighbourhood around the point of interest on the curve. We tested the accuracy on a discrete circle with a radius of 40 pixels using Bresenham's circle algorithm. The results can be seen in Figure 8. The Parameter k starts at $0.05 * n$ as the error gets too big for smaller values. As k increases we can see that the error gets smaller. The same is true for a constant k but an increasing radius, which corresponds to the multigrid convergence theorem, where we expect the accuracy to increase as the grid resolution (or in our case the circle radius) increases [7, Chapter 10].

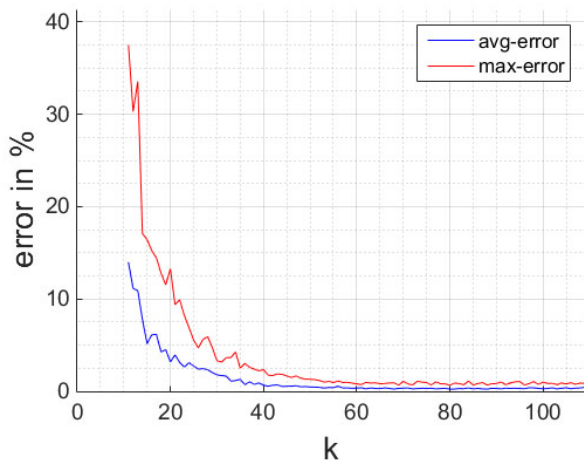


Figure 8. Plot of the avg- and max-error for the curvature estimation of a circle with radius 40 and increasing k .

So the accuracy gets better with increasing k . Unfortunately, this accuracy comes at a price, as

small curvatures are overlooked in the process if k is too big. Another problem with a fixed neighbourhood k are points at the beginning and the end of the skeleton curve. For points p_a with $a \leq k$ there are no neighbourhood points p_{a-k} defined, as the index would become null or negative. The same is true for points p_b with $b > n - k$ where no neighbourhood points p_{b+k} are defined, as the index would get bigger than n . We currently solve this problem by disregarding those points on the curve. In Figure 7 the curvature values always start at the index $1 + k$ and end at the index $n - k$. Another problem is the determination of a good value for the parameter k . In Figure 7 the blue line shows the curvature for $k = 17$ which equals $0.15 * n$ and gives the best results on the tested worms.

6.6. Normalized shape

We achieve the normalized shape representation of a worm with a backward medial axis transform approach. The starting point is the distance transform of the binary worm image which labels each pixel with the Euclidean distance to the nearest boundary in the binary image. For every point p_i of sorted list s of skeleton points, we use the coordinates to look up the distances in the distance transform. Those distances then serve as the radii for the circles. See Figure 9 for a visualization.

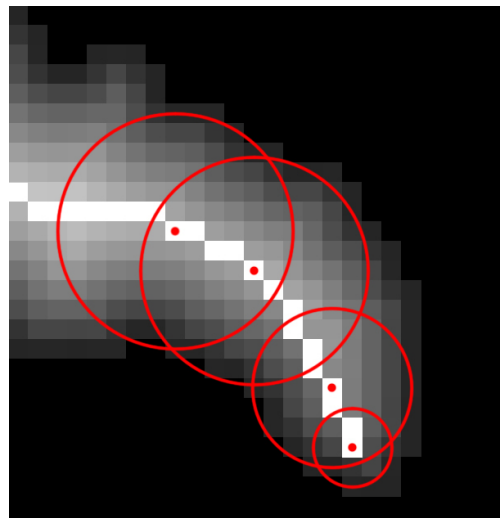


Figure 9. Part of the distance transform of a worm with circles drawn for four points on the skeleton.

To get a suitable representation of the worm, the distances between the skeleton points in the video frame need to stay the same on the normalized shape representation. Therefore the Euclidean distance

between the points is calculated and taken into account when drawing the circles. Figure 10 shows the results of this method, where in the first visualization only the outlines of a few circles are drawn to show the general idea behind this approach.

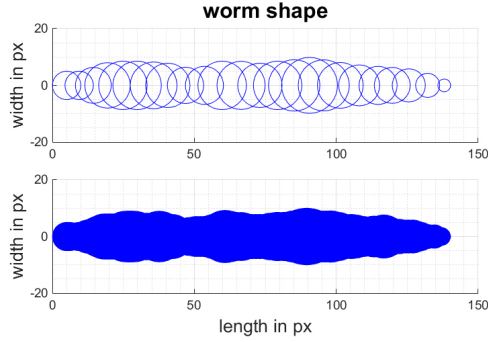


Figure 10. Plots of the normalized representation of a worm using only the outlines of 24 circles to visualize the general idea (top) and a complete shape visualization with all 115 filled circles (bottom) for that worm.

6.7. Length

To calculate the length of a worm, we use the geodesic distance of its skeleton plus the radii of the circles at the first and last skeleton point. The circle radii are needed as our skeleton endpoints do not lie at the edge of the worm. The geodesic distance is computed using the Euclidean distance.

6.8. Area

For the area of a worm, we simply calculate the sum of all foreground pixels of the binary image of the worm, which is the zeroth moment.

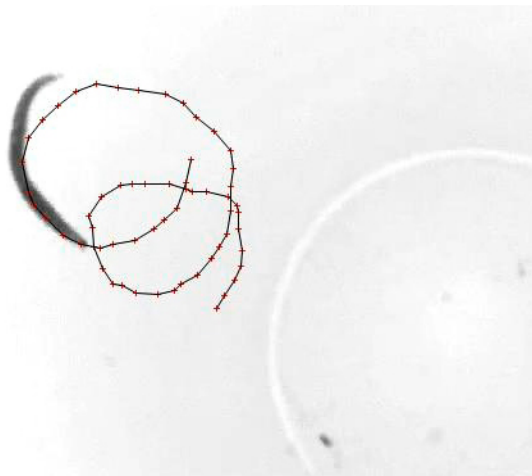


Figure 11. Part of a video frame with an overlay of the head trajectory. The trajectory is taken from a short sequence of a single worm video.

7. Single worm experiments

Some experiments with single female worm videos were conducted. Figure 12 shows two plots of smoothed worm lengths. For the smoothing a moving average filter was applied to the original data. The plots show the length of the worms around the time of the gamete release where the female worms secrete their eggs into the water and get smaller and therefore shorter. This can also be observed in the plots.

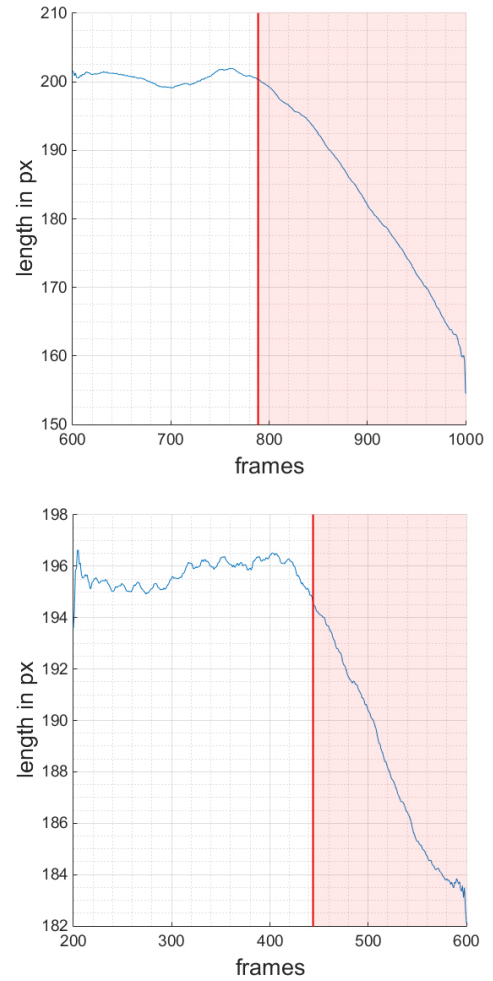


Figure 12. Two plots of smoothed worm lengths for two different female worms right around the time of the gamete release (marked in red).

Figure 13 shows how the length of a female worm changes during an entire spawning process. Annotation A marks a special case where the worm is overlapping itself resulting in a faulty binary area and skeleton. The problem here is the 3D movement of the worm.

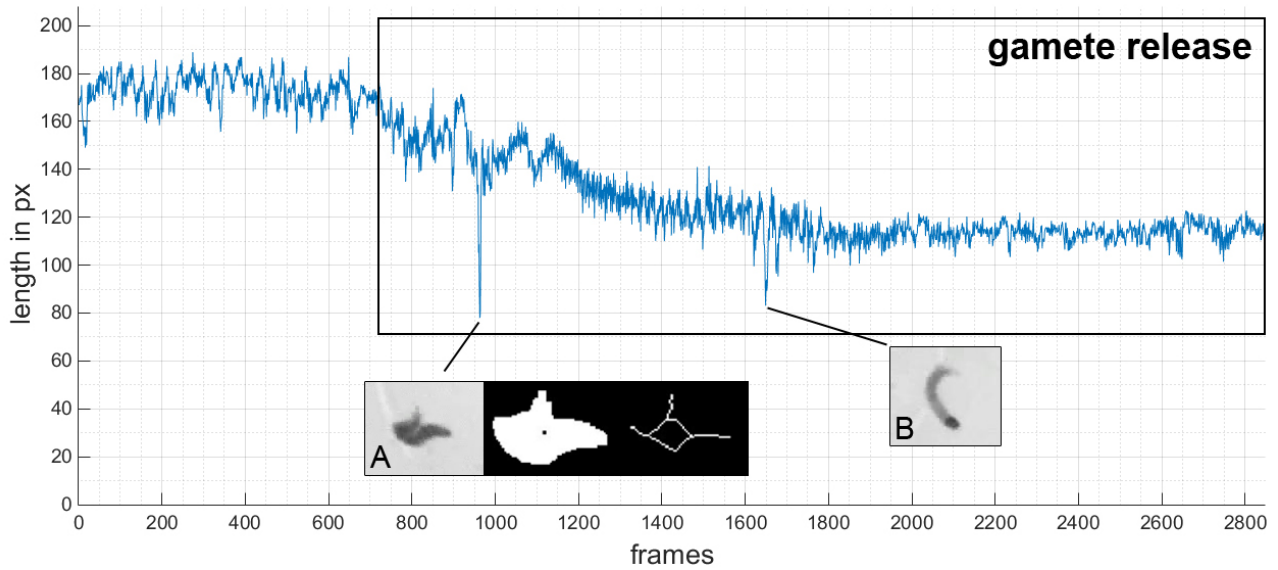


Figure 13. Change of worm length over time. During the gamete release the worm gets shorter. Annotation A: Wrong skeleton due to 3D movement of the worm. Annotation B: Wrong length due to 3D movement of the worm.

Another special case where the 3D movement also results in error-prone data is marked with annotation *B*. Here the end of the tail is not visible to the camera which makes the worm appear shorter in the video.

8. Conclusion and Future work

In this paper we proposed a novel worm tracking approach for *Platynereis dumerilii* worms, that enables both tracking and feature extraction from captured videos. Although our tracking approach is not suitable for tracking two worms in difficult cases our methods to extract worm features already show promising results.

The method we currently use to track single worms works for two worms if they are physically separated, but as they get close to each other or overlap, the current method might fail. In the future, we will extend the method to consider cases where the worms are close to each other or even overlap. Ideas to achieve this include the comparison of more features than just the head positions of consecutive frames. A combination of all other features could yield an appropriate approach in distinguishing male and female worms.

The current feature extraction is robust in most cases, but there exist special cases, where a single worm overlaps itself due to 3D movement in the water. This results in regions and skeletons, which do not represent the worm correctly and therefore the

extracted features are flawed as well. One approach will be to look into the watershed method to segment the worms as it might be superior to the simple threshold based method we use now, especially for worms that overlap.

Our approach to compute the curvature also has some flaws and is not robust enough. In the future we will look into alternative approaches to compute the curvature of discrete curves. Other methods that try to estimate the osculating circles rely on digital straight segments (DSS) recognition [6] [4] and Roussillon and Lachaud [9] base their method around maximal digital circular arcs.

9. Acknowledgement

The research leading to these results has received funding from the European Research Council under the European Community's Seventh Framework Programme (FP7/2007-2013)/ERC Grant Agreement 337011 to KT-R.

We also thank the anonymous reviewers for their valuable input.

References

- [1] N. Aigerman, R. Poranne, and Y. Lipman. Lifted bijections for low distortion surface mappings. *ACM Trans. Graph.*, 33(4):69:1–69:12, July 2014. 2
- [2] J. B. Arous, Y. Tanizawa, I. Rabinowitch, D. Chatenay, and W. R. Schafer. Automated imaging of neuronal activity in freely behaving

- caenorhabditis elegans. *Journal of Neuroscience Methods*, 187(2):229 – 234, 2010. 3
- [3] J. Casey. *A sequel to the first six books of the elements of Euclid, containing an easy introduction to modern geometry, with numerous examples*. 7th edition, revised and enlarged. Dublin. Hodges. University Press Series. 184 S, (1895). 5
 - [4] D. Coeurjolly, S. Miguet, and L. Tougne. Discrete Curvature based on Osculating Circles Estimation, 2001. 4th International Workshop on Visual Form 2001, Capri, Italy, Springer Lecture Notes in Computer Science 2059, pages 303-312. 8
 - [5] A. Gray. *Modern Differential Geometry of Curves and Surfaces with Mathematica*. CRC Press, Inc., Boca Raton, FL, USA, 1st edition, 1996. 5
 - [6] S. Hermann and R. Klette. A comparative study on 2d curvature estimators. In *Computing: Theory and Applications, 2007. ICCTA '07. International Conference on*, pages 584–589, March 2007. 5, 8
 - [7] R. Klette and A. Rosenfeld. *Digital Geometry*. Morgan Kaufman Publishers, 2004. 6
 - [8] D. Ramot, B. E. Johnson, T. L. Berry, Jr, L. Carnell, and M. B. Goodman. The parallel worm tracker: A platform for measuring average speed and drug-induced paralysis in nematodes. *PLoS ONE*, 3(5):e2208, 05 2008. 3
 - [9] T. Roussillon and J.-O. Lachaud. Accurate curvature estimation along digital contours with maximal digital circular arcs . In *14-th International Workshop on Combinatorial Image Analysis (IWCIA)*, LNCS, pages 43–55. Springer, 2011. 8
 - [10] G. D. Tsibidis and N. Tavernarakis. Nemo: a computational tool for analyzing nematode locomotion. *BMC Neuroscience*, 8(1):1–7, 2007. 3
 - [11] F. Ying. *Visual ants tracking*. PhD thesis, University of Bristol, 2004. 3